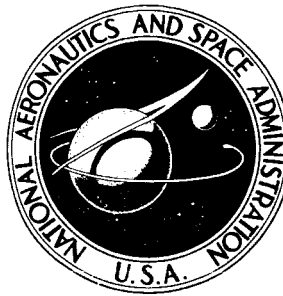


**NASA TECHNICAL
MEMORANDUM**



NASA TM X-1539

NASA TM X-1539

GPO PRICE \$ _____

CFSTI PRICE(S) \$ _____

Hard copy (HC) 300

Microfiche (MF) 65

ff 653 July 65

FACILITY FORM 602

| | |
|-------------------------------|------------|
| (ACCESSION NUMBER) | (THRU) |
| <u>34</u> | <u>1</u> |
| (PAGES) | (CODE) |
| (NASA CR OR TMX OR AD NUMBER) | (CATEGORY) |

**GAMMA FLUX AND HEAT DEPOSITION
IN PLUM BROOK REACTOR - COMPARISON
OF CALCULATION AND EXPERIMENT**

by Robert J. Bacigalupi and Byron E. Thinger

Lewis Research Center

Cleveland, Ohio

GAMMA FLUX AND HEAT DEPOSITION IN PLUM BROOK
REACTOR - COMPARISON OF CALCULATION
AND EXPERIMENT

By Robert J. Bacigalupi and Byron E. Thinger

Lewis Research Center
Cleveland, Ohio

NATIONAL AERONAUTICS AND SPACE ADMINISTRATION

For sale by the Clearinghouse for Federal Scientific and Technical Information
Springfield, Virginia 22151 - CFSTI price \$3.00

GAMMA FLUX AND HEAT DEPOSITION IN PLUM BROOK REACTOR - COMPARISON OF CALCULATION AND EXPERIMENT

by Robert J. Bacigalupi and Byron E. Thinger

Lewis Research Center

SUMMARY

A computerized point-kernel technique (QAD-P5) was used to calculate a gamma-heating map of a thermionic diode experiment proposed to be irradiated in the Plum Brook reactor core. A replica of the diode was used in the low-power mockup reactor at Plum Brook to generate corresponding gamma-heating maps experimentally using lithium fluoride dosimetry. A detailed comparison of experimental and calculated values generally showed agreement to within ± 25 percent. Proper interpretation of the measured values is discussed herein.

INTRODUCTION

In the design of any inpile experiment the effect of gamma heating must be considered in order to eliminate the possibility of malfunction or even catastrophic failure due to overheating. In the case of the irradiation experiment described herein, gamma heating is the primary source of heat in a thermionic diode. Since direct measurements of gamma heating are not available in regions of high gamma flux, a FORTRAN IV point-kernel computation (QAD-P5) was employed to calculate gamma heating. This method supplies a complete flux mapping of the entire experiment and takes into account variations in the gamma source and self-shielding of experiment parts. Calculated results are compared with experimental measurements made on the same target in a low-power mockup of the test reactor.

The experiment (Plum Brook identification No. 66-02) for which the calculations and measurements were made involved the irradiation of a thermionic diode to ascertain the effect of gamma dose rate on the operating characteristics of the diode. Figure 1 presents a cross section of the diode viewed from the top of the core. The diode consists primarily of the hot emitter ($\sim 2000^{\circ}\text{K}$) separated from the cooler collector ($\sim 1000^{\circ}\text{K}$)

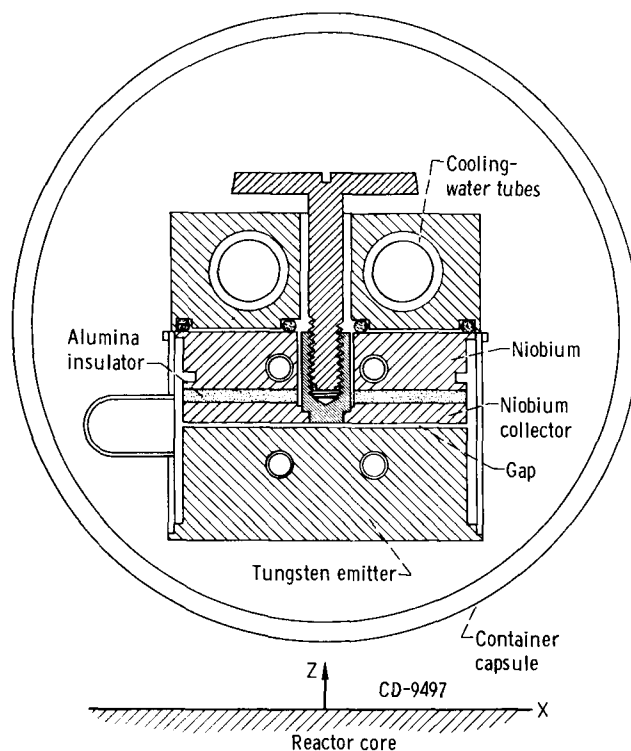


Figure 1. - Proposed thermionic diode (top view).

by 0.025-centimeter gap which is filled with cesium or another appropriate gas at low pressure. The emitter and collector are mechanically attached by the skirt which serves as a heat choke and as containment for the cesium. Gamma heating in the emitter and collector serves as the heat source to these parts so the gamma-heat input must be balanced against the heat rejection to allow each part to operate at its predetermined temperature.

Gamma flux alters the diode performance possibly by changing the conductivity of the plasma in the diode gap. Plasma conductivity is altered by the ion pairs which are continually being produced in the interelectrode gap by the secondary electrons initiated by gamma interaction with the electrode surfaces. Effects similar to these are reported in references 1 and 2. The study reported herein had two purposes: (1) to determine gamma heating for heat-transfer considerations and (2) to determine gamma dose rate in the diode gap so that it could be used as the parameter for study.

Since gamma dose rate was the primary parameter to be studied, the irradiation experiment was designed so that the diode could operate under the same conditions of temperature and filling gas pressure while varying the gamma flux. This was accomplished by providing variable cooling to the emitter, collector, and cesium reservoir while allowing the entire experiment to be moved vertically within the core hole to different gamma flux levels.

Of primary concern is the gamma heating in the emitter since the emitter is made of tungsten (high energy-absorption cross section) and is the furthest removed from cooling water. The collector is also of some importance since niobium has a relatively high energy-absorption cross section and is not directly thermally coupled to cooling water. The remainder of the parts are closely enough coupled to water cooling and of sufficiently low density so that exact gamma-heating values are not required.

MOCKUP REACTOR DOSIMETER EXPERIMENT

Experiment Capsule

A nuclear mockup of the intended diode was inserted into the mockup reactor (see the section Source Description for location) at Plum Brook in order to measure directly

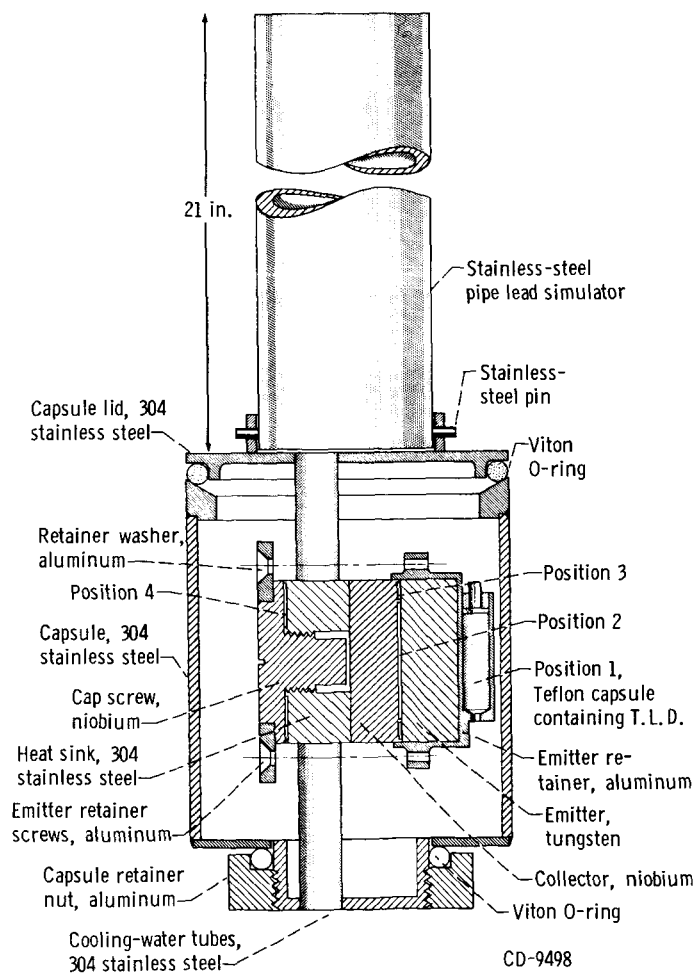


Figure 2. - Experiment assembly for mockup reactor gamma test.

gamma heating in situ in certain strategic positions in the diode. A detailed mapping of gamma heating in the diode, such as is available by calculation, is not practical by dosimetry because of the finite-size body of the dosimeters and the time necessary for each measurement.

Two identical capsules (illustrated in fig. 2) were fabricated in order to decrease the wait for radiation cooling-off between runs. Figure 3 is a closeup side view of the

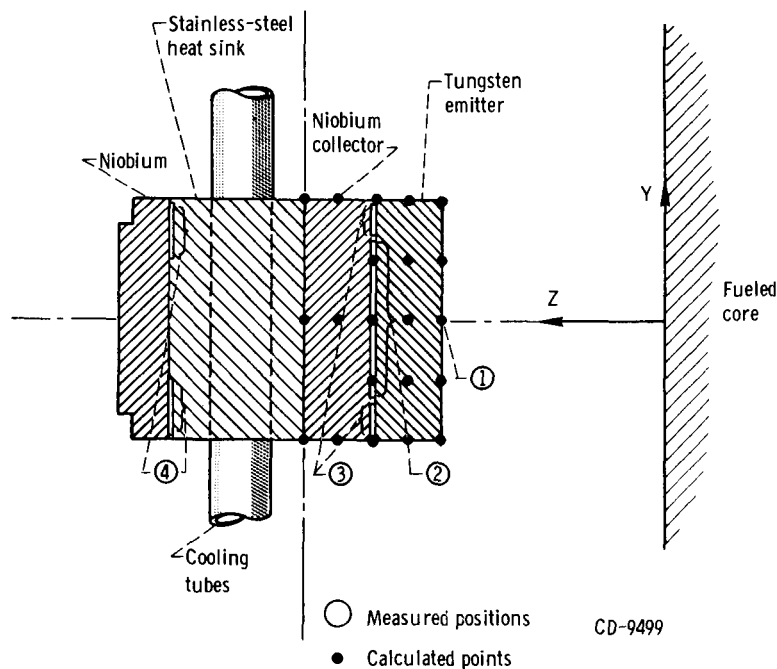


Figure 3. - Nuclear mockup of thermionic diode.

dosimeter cavities. The areas in figure 3 numbered 1 to 4 indicate locations at which thermoluminescent dosimeter material (T. L. D.), Li^7F , was placed to measure gamma heating. At position 1, a Teflon capsule filled with T. L. D. was secured against the outside of the emitter to measure incident flux. Positions 2 and 3 are concentric disk-shaped cavities approximately 0.025 centimeter deep filled with T. L. D. which is arranged to allow a measurement of the radial attenuation in the gap. A similar cavity at position 4 allows the attenuation in the remaining material in the diode to be evaluated.

Thermoluminescent Dosimetry

Gamma-heating values were measured in the mockup reactor experiment by using the thermoluminescent property of doped lithium 7 fluoride (Li^7F) crystals. A complete

description of the physical mechanism appears in reference 3, while a good description of the technique is presented in reference 4. A brief description of both follows.

Incident gamma radiation in the energy range of interest (0.5 to 3 MeV or 0.801×10^{-13} to 4.806×10^{-13} J) interacts with matter primarily by Compton scattering, which results in an energetic electron and a scattered photon of lower than incident energy. Energy deposition takes place as the electron scatters around in the target material and undergoes a multitude of energy-degrading interactions with electrons and nuclei within a short distance of the Compton collision (of the order of 0.01 cm for W and 0.08 cm for LiF) (ref. 5).

Impurities and imperfections in the LiF crystals produce metastable trap states between the valence and conduction bands. Electrons excited from the valence band into these trap states remain trapped indefinitely at room temperature, but, when the temperature of the LiF is raised, the half-life for recombination of trapped electrons with valence holes decreases exponentially to the order of seconds at 300° C. The energy for excitation comes from high-energy electrons produced by Compton scattering in material immediately surrounding the T. L. D. In recombining, the trapped electrons give off photons of energy equal to the various trap depths, which in this case is in the range of visible light. For properly annealed LiF the light output is linearly proportional to total dose to a known saturation level, which is, of course, avoided. The light output of the T. L. D. material is calibrated against a known source strength of cobalt 60 gammas. Since the response of T. L. D. to incident energies from 30 KeV (0.04806×10^{-13} J) to greater than 1.2 MeV (1.922×10^{-13} J) has been measured to be essentially flat, the calibration is valid even though the incident-energy distribution in calibration and experiment are different.

The use of T. L. D. powder containing 99.99 percent Li^7 eliminated the thermal-neutron response of Li^6 . However, the effect of neutron heating in the materials immediately adjacent to the T. L. D. (by (n, γ) reactions) is recorded in the T. L. D. through the chain of events just described except, of course, that the source of gammas is an (n, γ) reaction rather than core fission. The (n, γ) contribution is treated more fully later in a separate section.

Experimental Results

Measurements in the mockup reactor were made for beginning-of-life (BOL) and end-of-life (EOL) core conditions with the diode at three vertical positions in LA-7. Beginning-of-life refers to the beginning of the reactor cycle when the movable rods are about half inserted into the core. These rods are continuously removed during reactor operation to compensate for burnup until at the end-of-life when they are fully removed. The difference in the gamma source form for these two core conditions is illustrated by the

difference in the power distribution curves for BOL and EOL in the appendix. The mock-up reactor was operated at 250 to 300 watts to preclude saturation of the T. L. D. dosimeter material. The results of the mockup reactor dosimeter experiment as summarized in table I (unpublished data obtained from Nuclear Support Branch of Plum Brook Station) are scaled to the 60-megawatt power level of the Plum Brook reactor.

TABLE I. - GAMMA-HEATING VALUES

[Measured in LA-7 of mockup reactor using Li^7F dosimeters.]

| Core operating mode | Emitter thickness, cm | Gamma heat, W/g, at position - | | | | Diode vertical position above core centerline | |
|---------------------|-----------------------|--------------------------------|-------|-------|-------|---|------|
| | | 1 | 2 | 3 | 4 | in. | cm |
| | | | | | | | |
| BOL | 2/3 | 11.98 | 11.60 | 12.43 | 9.67 | 0 | 0 |
| | 2/3 | 9.20 | 8.16 | 8.90 | 7.41 | 4 | 10.2 |
| | 2/3 | 5.32 | 4.90 | 5.54 | 4.50 | 8 | 20.3 |
| | 1/3 | 12.24 | 12.58 | 12.82 | 9.88 | 0 | 0 |
| | 1 | 12.63 | 7.74 | 9.35 | 10.35 | 0 | 0 |
| EOL | 2/3 | 12.59 | 10.34 | 11.26 | 10.26 | 0 | 0 |
| | 2/3 | 11.06 | 9.15 | 9.96 | 9.91 | 4 | 10.2 |
| | 2/3 | 8.95 | 7.43 | 8.41 | 7.33 | 8 | 20.3 |

QAD-P5 CALCULATION

Method

QAD-P5 is a FORTRAN IV computer program (IBM 7094-II, 32K) written at Los Alamos Scientific Laboratory to calculate gamma- and fast-neutron radiation fluxes from a volume-distributed source. A detailed account of the computer code can be found in reference 6. The program has been modified at Lewis to include tables of gamma total cross sections, neutron-removal cross sections, parameters for infinite medium buildup factors, and several gamma response functions. Reference 7 describes these libraries and lists the sources from which the data were taken.

The method of calculation of gamma flux and local heating rates proceeds on the basis of the attenuation of a line-of-sight gamma beam from a point-kernel source to a prescribed receiver point. In addition to the geometric $1/4\pi r^2$ attenuation, the gamma beam traverses regions that have material composition where attenuation is dependent on the gamma mass-absorption coefficient and the mass thickness of the element encountered between the source point and the receiver point. In each ray trace, a tally is kept of the geometric distance traveled in a region and the points of intersections with the boundaries

which specify the regions. At the receiver point, the attenuated direct-beam flux is multiplied by a buildup factor, which is representative of the material and distance traversed, to account for scattered gamma radiation. The resulting total flux is then multiplied by the proper gamma energy-absorption coefficient to determine the gamma-heating rate.

Neutron-heating rates due to elastic collisions of fast neutrons with nuclei were calculated from curve-fit data to the infinite-medium-momentum method, but these rates proved insignificant in this case.

Source Description

The fueled core of the Plum Brook reactor and its mockup is composed of twenty-seven 3- by 3- by 24-inch elements arranged in a lattice (top view shown in fig. 4). Because of the rectangular geometry, Cartesian coordinates were used to specify rela-

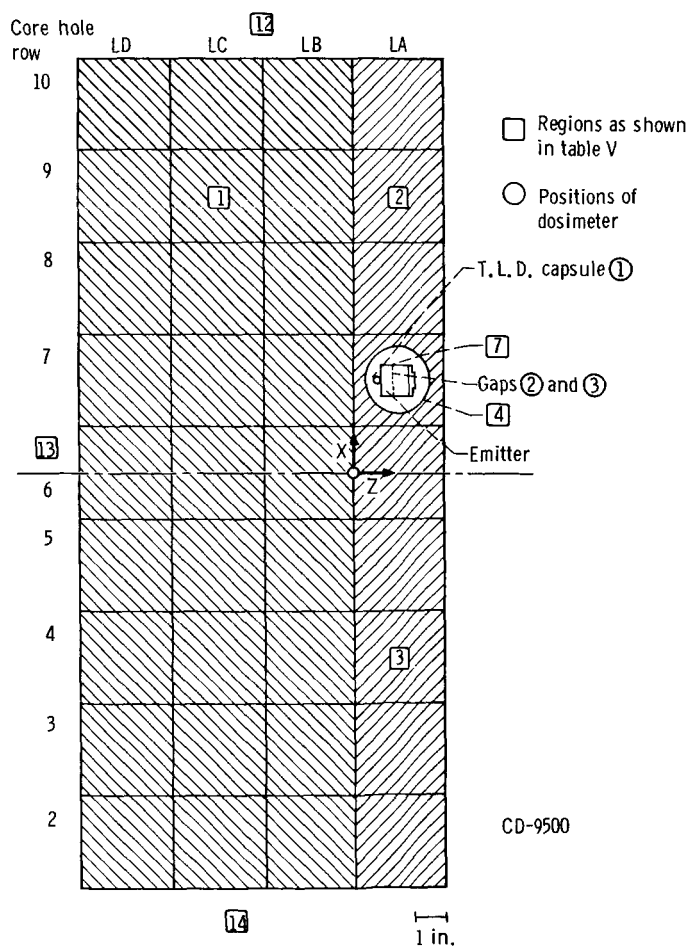


Figure 4. - Plum Brook core with diode in place (top view).

tive fission distributions. The core horizontal midplane, $X = 0$, the core vertical midplane, $Y = 0$, and the fueled core boundary (that closest to the experiment site), $Z = 0$, identify the origin of the coordinate axes. A volume-distributed source was obtained by dividing the core volume into 18 by 19 by 10 equal volumes and calculating the relative source intensity from prescribed X, Y, Z fission-distribution functions at the center of each volume element. The particular fission-distribution functions used in this computer program are shown in figures 5 and 6. Since the measured power distribution in the Z -direction is nearly flat, it was assumed to be flat for this calculation. The source

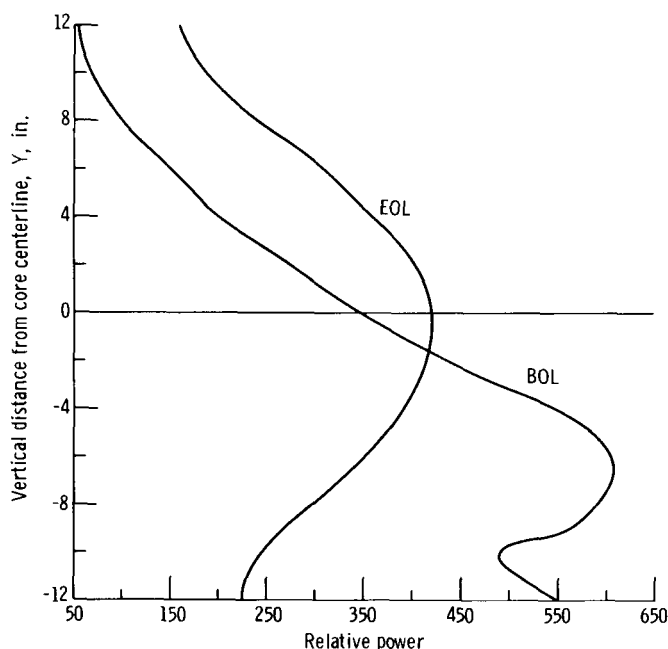


Figure 5. - Vertical relative power distribution in LB-7 as function of vertical distance from core centerline.

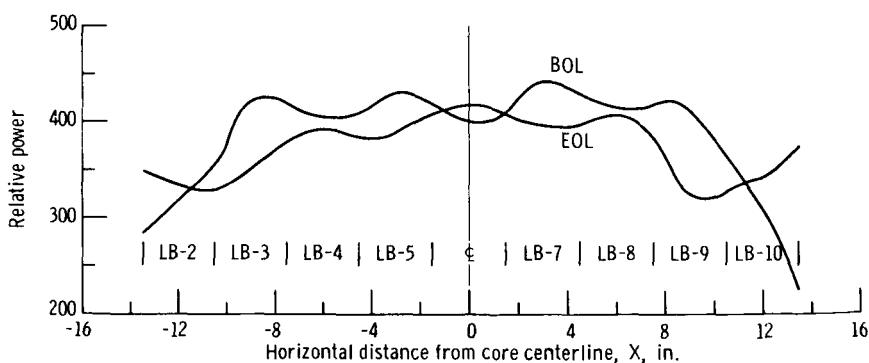


Figure 6. - Horizontal relative power distribution for mockup reactor D as function of horizontal distance from core centerline.

TABLE II. - PROMPT AND DELAY GAMMA ENERGY SPECTRUM

(a) U. S. Customary Units

| Energy group, MeV | Gamma energy release per fission, MeV/fission | Mean gamma energy, MeV |
|----------------------|---|------------------------------|
| 0.1 to 0.4 | 0.723 | 0.267 |
| 0.4 to 0.9 | 2.74 | .618 |
| 0.9 to 1.35 | 2.54 | 1.119 |
| 1.35 to 1.8 | 2.09 | 1.572 |
| 1.8 to 2.2 | 1.62 | 1.995 |
| 2.2 to 2.6 | 1.23 | 2.394 |
| 2.6 to 3.0 | 1.05 | 2.792 |
| 3.0 to 3.5 | .96 | 3.235 |
| 3.5 to 4.0 | .696 | 3.74 |
| 4.0 to 4.5 | .502 | 4.228 |
| 4.5 to 5.0 | .322 | 4.735 |
| 5.0 to 5.5 | .212 | 5.23 |
| 5.5 to 8.0 | .338 | 6.334 |

(b) SI Units

| Energy group, J | Gamma energy release per fission, J/fission | Mean gamma energy, J |
|--|---|----------------------------|
| 0.1602×10^{-13} to 0.6408×10^{-13} | 1.158×10^{-13} | 0.427×10^{-13} |
| 0.6408 to 1.442 | 4.389 | .990 |
| 1.442 to 2.162 | 4.069 | 1.792 |
| 2.162 to 2.883 | 3.348 | 2.518 |
| 2.883 to 3.524 | 2.595 | 3.196 |
| 3.524 to 4.165 | 1.970 | 3.835 |
| 4.165 to 4.806 | 1.682 | 4.472 |
| 4.806 to 5.607 | 1.538 | 5.182 |
| 5.607 to 6.408 | 1.115 | 5.991 |
| 6.408 to 7.209 | .804 | 6.773 |
| 7.209 to 8.010 | .516 | 7.585 |
| 8.010 to 8.811 | .340 | 8.378 |
| 8.811 to 12.816 | .541 | 10.147 |

TABLE III. - (n, γ) CORE CAPTURE GAMMA ENERGY SPECTRUM

(a) U. S. Customary Units

| Energy group, MeV | Gamma energy release per capture, MeV/capture | Gamma energy release per fission (modified), MeV/fission | Mean gamma energy, MeV |
|--|---|---|------------------------------|
| 0.1 to 0.4 | 0 | 0.001 | 0.267 |
| 0.4 to 0.9 | 0 | .001 | .618 |
| 0.9 to 1.35 | 1.78 | .001 | 1.119 |
| 1.35 to 1.8 | 0 | .155 | 1.572 |
| 1.8 to 2.2 | 2.23 | .001 | 1.995 |
| 2.2 to 2.6 | 0 | .453 | 2.394 |
| 2.6 to 3.0 | ↓ | .001 | 2.792 |
| 3.0 to 3.5 | | ↓ | 3.235 |
| 3.5 to 4.0 | | | 3.74 |
| 4.0 to 4.5 | | | 4.228 |
| 4.5 to 5.0 | | | 4.735 |
| 5.0 to 5.5 | ↓ | | 5.23 |
| 5.5 to 8.0 | 7.72 | .230 | 6.334 |
| Total gamma energy release per fission | | 0.848 | |

(b) SI Units

| Energy group, J | Gamma energy release per capture, J/capture | Gamma energy release per fission (modified), J/fission | Mean gamma energy, J |
|--|---|---|----------------------------|
| 0.1602×10^{-13} to 0.6408×10^{-13} | 0 | 0.0016×10^{-13} | 0.427×10^{-13} |
| 0.6408 to 1.442 | 0 | .0016 | .990 |
| 1.442 to 2.162 | 0 | .0016 | 1.792 |
| 2.162 to 2.883 | 2.851×10^{-13} | .2483 | 2.518 |
| 2.883 to 3.524 | 0 | .0016 | 3.196 |
| 3.524 to 4.165 | 3.572×10^{-13} | .7257 | 3.835 |
| 4.165 to 4.806 | 0 | .0016 | 4.472 |
| 4.806 to 5.607 | ↓ | ↓ | 5.182 |
| 5.607 to 6.408 | | | 5.991 |
| 6.408 to 7.209 | | | 6.773 |
| 7.209 to 8.010 | | | 7.585 |
| 8.010 to 8.811 | | | 8.378 |
| 8.811 to 12.816 | 12.367×10^{-13} | .3684 | 10.147 |
| Total gamma energy release per fission | | 1.358 | |

strength at each source point (3420 points) was calculated from the normalized X, Y, Z source distribution. Normalization is with respect to the total source strength, which is 3.3×10^{10} fissions per second per watt times the operating power level of the reactor (in this case, 60 MW). The prompt gamma-energy release per fission is 7.82 MeV (12.527×10^{-13} J). The decay gamma contribution used is 7.203 MeV (11.54×10^{-13} J) per fission. There are several references which specify fission gamma-energy spectrums (refs. 8 to 11). However, the Groshev experimental energy spectrum given in reference 11 was used because of similarities in reactor geometry and material composition. Included in this spectrum are the contributions of prompt gammas, decay gammas, and (n, γ) core capture gammas. The noticeable spikes that depict the (n, γ) capture spectrum for hydrogen and aluminum are subtracted from the experimental spectrum so that they may be dealt with separately. Table II indicates how the modified gamma spectrum (prompt plus decay gammas only) is broken into 13 energy groups to give an energy distribution which is normalized with respect to a total energy release of 15.023 MeV (24.066×10^{-13} J) per fission. The source strength for the $H^1(n, \gamma)H^2$ reaction is equal to the number of thermal neutrons captured in water per fission times the number of fissions per second. The source strength for the $(n, \gamma)Al^{27}$ reaction is similarly proportional to the number of thermal-neutron captures occurring in aluminum per fission. The gamma energy release in the H^1 reaction is 2.23 MeV (3.572×10^{-13} J) per capture, whereas in the latter reaction there is a gamma energy spectrum ranging from 1 to 7.72 MeV (1.602×10^{-13} to 12.367×10^{-13} J). Only those gammas at 7.72 MeV (12.367×10^{-13} J) were considered, however, because the prompt and decay gamma spectrum is predominant at the lower energies. There is an additional 1.78-MeV (2.852×10^{-13} -J) gamma energy release in beta decay of Al^{28} , which is included in the complete (n, γ) core capture spectrum. Table III describes this spectrum.

Two sets of fission-distribution functions are used in the computer program; one set portrays the thermal power at reactor startup (or BOL) and the other portrays the thermal power at the end of the reactor cycle (or EOL). For both these cases, the fuel loading, designated MUR-D, is described in table IV.

Geometry and Material Composition

The QAD-P5 mockup of the Plum Brook reactor and Lewis nuclear thermionic diode is shown in figure 4. The boundaries of the various regions are described by quadratic equations. In this geometry, the fueled core is the source volume and is assumed to be a homogeneous mixture of stainless steel, aluminum, water, cadmium, and enriched uranium. The unfueled portion of the core is assumed to be a homogeneous mixture of beryllium and water. The emitter and collector of the diode are tungsten and niobium, re-

TABLE IV. - PLUM BROOK REACTOR

D FUEL LOADING

| Column | Row | | | | | | | | |
|--------|----------------------------|-----|-----|-----|-----|-----|-----|-----|-----|
| | 2 | 3 | 4 | 5 | 6 | 7 | 8 | 9 | 10 |
| | U ²³⁵ weight, g | | | | | | | | |
| LB | 200 | 168 | 168 | 135 | 135 | 135 | 168 | 168 | 200 |
| LC | 155 | 240 | 130 | 135 | 130 | 135 | 130 | 240 | 155 |
| LD | 200 | 168 | 168 | 135 | 135 | 135 | 168 | 168 | 200 |

TABLE V. - DENSITY COMPOSITION MATRIX

| Composition | Region | ¹ H ¹ | ⁴ Be ⁹ | ⁸ O ¹⁶ | ¹³ Al ²⁷ | ²⁴ Cr ⁵² | ²⁶ Fe ⁵⁶ | ²⁸ Ni ⁵⁹ | ⁴¹ Nb ⁹³ | ⁴⁸ Cd ¹¹² (a) | ⁷⁴ W ¹⁸⁴ | ⁹² U ²³⁵ |
|-------------------|-----------------------|-----------------------------|------------------------------|------------------------------|--------------------------------|--------------------------------|--------------------------------|--------------------------------|--------------------------------|--|--------------------------------|--------------------------------|
| | | Density, g/cm ³ | | | | | | | | | | |
| Core | 1 | 0.065 | 0 | 0.520 | 1.08 | 0.0313 | 0.113 | 0.0244 | 0 | 0.0485 | 0 | 0.0461 |
| Beryllium lattice | 2, 3 | .0116 | 1.89 | .093 | 0 | 0 | 0 | 0 | 0 | 0 | 0 | 0 |
| LA7 channel | 4 | 0 | 0 | 0 | 2.7 | 0 | 0 | 0 | 0 | 0 | 0 | 0 |
| Water | 5, 6 | .111 | 0 | .889 | 0 | 0 | 0 | 0 | 0 | 0 | 0 | 0 |
| Void ^b | 7, 8, 11, | 0 | 0 | 0 | 0 | 0 | 0 | 0 | 0 | 0 | 0 | 0 |
| | 12, 13, 14, 15, 16 | | | | | | | | | | | |
| Emitter | 9 | 0 | 0 | 0 | 0 | 0 | 0 | 0 | 0 | 0 | 19.3 | 0 |
| Collector | 10 | 0 | 0 | 0 | 0 | 0 | 0 | 0 | 8.4 | 0 | 0 | 0 |

^aCadmium volume fraction in core changes with fuel-rod insertion; these numbers are representative of BOL.

^bAll external regions and those not between source volume and detector point are considered as void.

spectively. Table V shows the element composition of each region in terms of partial density and atomic number. Libraries of gamma mass-attenuation coefficients and neutron-removal cross sections for all elements are internal in the computer code. In ray trace calculations, the appropriate attenuation factors are used according to the composition specification of a particular region.

Receiver

Figure 3 is a cross-sectional side view of the QAD configuration of the thermionic diode showing points at which the gamma-heating values are calculated in the Y, Z plane. The arrangement of five receiver points along the Y-axis is repeated along the X-axis so that heating-rate profiles could be sketchd for several X, Y planes in the emitter and collector. From total gamma-heat input and heat-transfer considerations, the temperature distribution in the diode may be calculated. Three sizes of tungsten emitters were evaluated: 1/3, 2/3, and 1 centimeter thick, all 2.5 centimeters in diameter. The 2/3-centimeter-thick emitter was analyzed more thoroughly for the sake of comparison to the measured value, which used primarily a 2/3-centimeter-thick emitter.

Computer Output and Results

Gamma-heating rate at a receiver point is determined by multiplying the total gamma energy flux in MeV per square centimeter per second ($J/(cm^2)(sec)$) by the appropriate gamma energy-absorption coefficient in square centimeters per gram for the

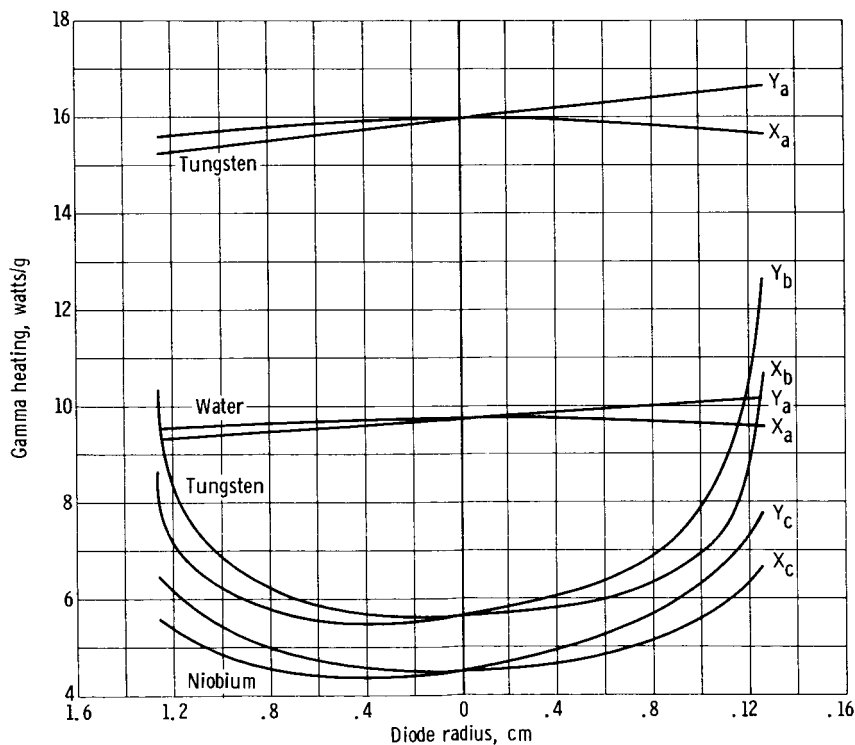


Figure 7. - Variation of calculated gamma heating as function of emitter radius for BOL core conditions with emitter at core centerline (n, γ in tungsten not included).

particular material in which the receiver point is located. A simple conversion factor of 1.6×10^{-13} changes the units to watts per gram.

A typical plot of computer output information is shown in figure 7 which illustrates gamma-heating profiles in the X, Y plane for various values of Z for the 2/3-centimeter emitter. The diode in this case is positioned at the vertical midplane of the reactor core. The particular Z-axis values of interest are coded by subscripts as follows: a, the front face of the emitter; b, the back of the emitter (or the gap); c, the middle plane of the collector. Heating rates in both water and in tungsten are presented for the front face of the emitter. This fact will be important when comparison is made between calculated and measured gamma-heating values. Figure 7 also displays the slight asymmetry of the Y-traces manifesting the asymmetry of the vertical fission distribution for BOL reactor operation. In this case, the bottom of the diode receives more gamma heating than the top. The X-traces, on the other hand, are fairly uniform and attributable to the close proximity of the diode to the reactor core horizontal mid-plane about which the fission distribution is symmetrical. As a comparison, figure 8 illustrates gamma-heating profiles in the same X, Y, Z planes as in figure 7, but here the profiles are symmetrical about the diode center, which is indicative of EOL reactor op-

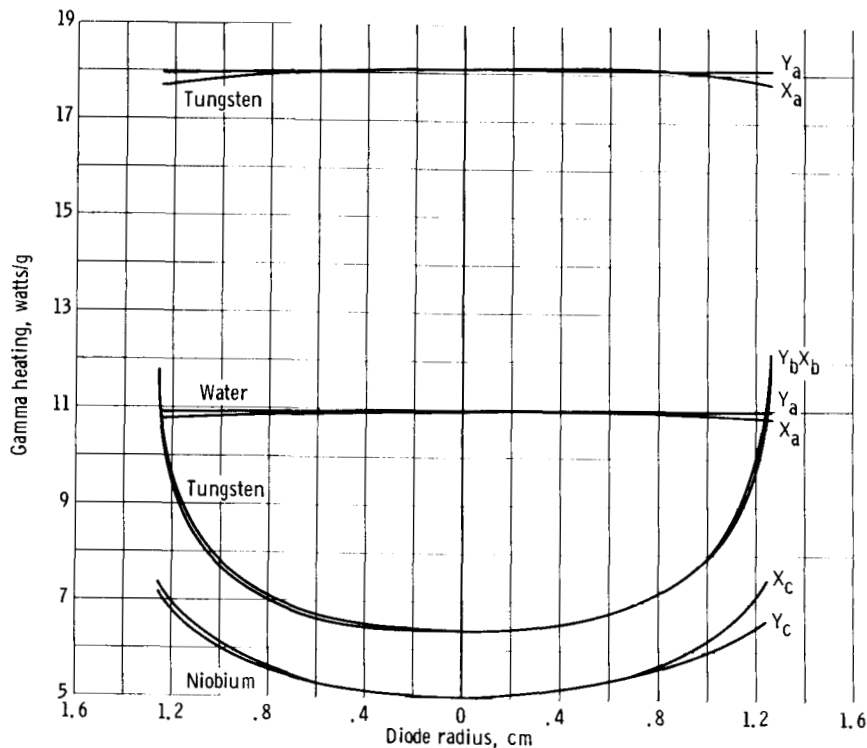


Figure 8. - Variation of calculated gamma heating as function of emitter radius for EOL core conditions with emitter at core centerline (n, γ in tungsten not included).

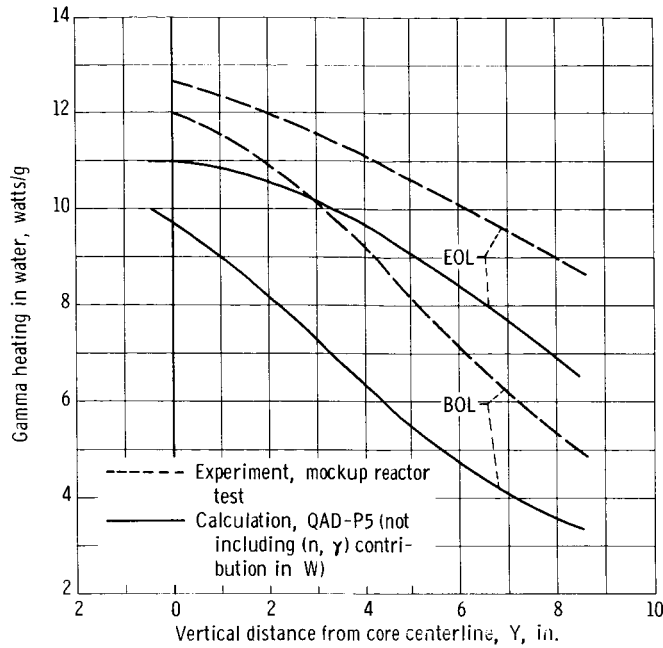


Figure 9. - Variation of gamma heating at position 1 with vertical distance from core centerline.

eration. The solid curves in figure 9 show the variation in gamma heating (excluding (n, γ) contribution) at the core side of the emitter as a function of diode vertical position in the core for both BOL and EOL conditions. For comparison, the dashed curves show the values as directly measured in the mockup reactor.

(n, γ) Contribution

As noted earlier, the measured values of gamma heating do include the effect of (n, γ) interactions in any high Σ material adjacent to the T. L. D. For a direct comparison between calculated and measured values of gamma heating, an estimated (n, γ) contribution must be added to the calculated values. One method of estimating the (n, γ) contribution at the core and gap sides of the emitter is as follows:

Method I:

Assuming beam geometry

$$Q_{n, \gamma} = \frac{1}{2} \Sigma_w \phi_{th} E_{\gamma} B \int_0^t \exp(-\mu Z) 1.6 \times 10^{-13} \frac{\mu_e}{\rho} dZ$$

where

| | |
|-----------------------|--|
| Σ_w | thermal n-capture cross section in tungsten, 1.21 cm^{-1} |
| E_γ | gamma energy produced per neutron capture, $6.5 \text{ MeV} (10.413 \times 10^{-13} \text{ J})$ |
| μ | total attenuation cross section for tungsten, 0.78 cm^{-1} |
| μ_e | energy-absorption cross section for tungsten, 0.65 cm^{-1} |
| t | emitter thickness, cm |
| 1.6×10^{-13} | $W/(\text{MeV})(\text{sec})$ |
| φ_{th} | thermal neutron flux, $N/(\text{cm}^2)(\text{sec})$ |
| B | buildup factor for 6.5-MeV (10.413×10^{-13} -J) gammas in tungsten, approximately 1.25 |

$$Q_{n,\gamma} = \frac{BK}{-\mu} \varphi \int_0^t \exp(-\mu Z) - \mu \, dZ$$

$$= \frac{KQ}{\mu} (1 - e^{-\mu t})$$

where $K = 1/2 \Sigma_w E_\gamma (\mu_e/\rho) 1.6 \times 10^{-13} = 2.22 \times 10^{-14}$ and B is estimated by extrapolating data in ANL-5800 (ref. 8) for 2/3 centimeter of tungsten:

$$Q_{n,\gamma} = \frac{2.22 \times 10^{-14}}{0.78} \varphi_{th}^{0.408} B$$

$$= 1.45 \times 10^{-14} \varphi_{th}$$

When measured values of φ_{th} as a function of vertical position Y are used, as shown in figure 10, where φ is independent of Z , $Q_{n,\gamma}$ may be calculated. Table VI which shows $Q_{n,\gamma}$ as a function of vertical height shows the contribution to be approximately 20 percent of the core gamma contribution at the gap.

Method II:

Another method of estimating (n, γ) heating is described here in which the total gamma generation from neutron capture in the entire test piece is multiplied by 1 minus the probability of escape of gammas from the test piece. This probability as obtained by a method described in reference 12 is 0.71.

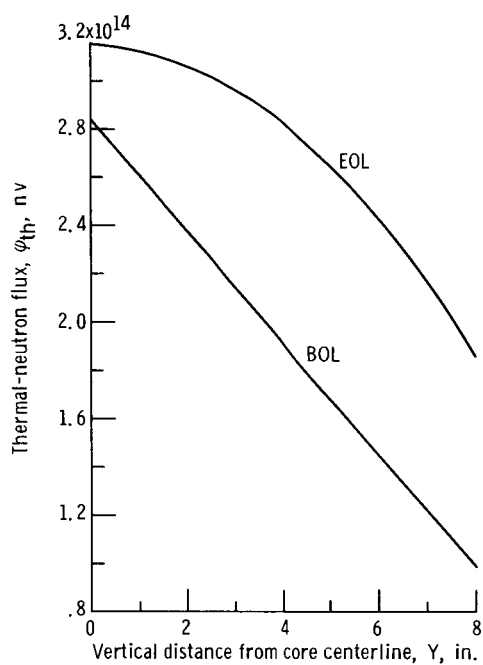


Figure 10. - Thermal-neutron flux, measured in LA-7 of mockup reactor corrected to 60 megawatts power, as function of vertical distance from core centerline.

TABLE VI. - (n, γ) CONTRIBUTION TO GAMMA HEATING IN A TWO-THIRDS-CENTIMETER TUNGSTEN EMITTER
AT BOTH GAP AND CORE SIDES

| Core condition | Diode elevation, in. | Method I (Beam geometry) | | Method II (Probability of escape) |
|----------------|----------------------|-----------------------------|-------------|--------------------------------------|
| | | Gamma heating, W/g | | Gamma heating in tungsten, W/g |
| | | In water | In tungsten | |
| BOL | 0 | 2.59 | 4.12 | 5.35 |
| | 4 | 1.75 | 2.77 | 3.60 |
| | 8 | .91 | 1.47 | 1.87 |
| EOL | 0 | 2.88 | 4.56 | 5.95 |
| | 4 | 2.58 | 4.10 | 5.35 |
| | 8 | 1.60 | 2.70 | 3.52 |

Therefore, average gamma heating in the entire test piece is

$$\begin{aligned}\tilde{Q} &= \Sigma \phi_{th} \frac{E_{\gamma}}{\rho} 1.6 \times 10^{-13} (1 - P) \\ &= 0.65 \times 10^{-13} 0.29 \phi_{th} \\ &= 1.89 \times 10^{-14} \phi_{th}\end{aligned}$$

Thermal flux values were taken from measurements made adjacent to the diode in the mockup reactor experiment. These values will produce high estimates in both methods since there will be some neutron attenuation in the tungsten due to capture. Values obtained by both methods are shown in table VI. Included in table VI is the (n, γ) heating estimated for the dosimeter material adjacent to the core side of the emitter. Since the dosimeter-material energy-absorption cross sections are approximately equal to those of water, the tungsten values were reduced by $\mu_{e, H_2O} / \mu_{e, W}$

Comparison of Results

Considering all sources of inaccuracy in both experiment and calculation, exact agreement between the two methods on absolute values of gamma heating should not be expected. However, good agreement should be realized in comparing relative values (e.g., incident/attenuated) so that the same trends are recognizable in both experiment and calculation. One point favoring the reliability of the calculational method is that its largest source of error, the buildup factor, was low (averaging between 2 and 3 in all cases). This results from the relatively small mass thickness of scatterer between the source and the detector.

A direct comparison was made between measurements and calculations at positions 1, 2, and 3 shown in figure 3 since these are the points of coincidences of the two methods. The calculated values must be area weighted over the regions in which the measurements were made since the calculations yield point-by-point heating data and the measurements yield heating values for finite regions. First, a curve of average gamma heating as a function of diode radius can be drawn (such as in fig. 11) for each situation by taking the average of four data points at equal radius from data curves (e.g., figs. 5 and 6). From these curves an area-weighted average gamma heating can be determined for positions 2 and 3 by a method described in the appendix.

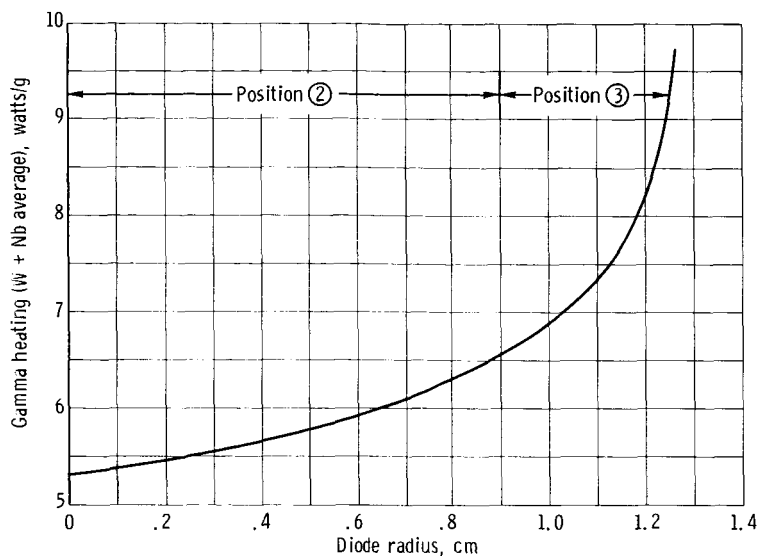


Figure 11. - Calculated gamma heating in tungsten plus niobium at gap side of 2/3-centimeter emitter for EOL core conditions with diode at core centerline as function of emitter radius.

To obtain a direct comparison, the physical mechanism of LiF dosimetry must be considered carefully. At position 1, T. L. D. was contained in a Teflon capsule which was held in place against the emitter by an aluminum holder (see fig. 2). Since the T. L. D. records the effect of Compton electrons produced in the material within the range of the electrons around the powder (ref. 13), the heating measured at position 1 is representative of (n, γ) heating in LiF, Teflon, and aluminum, all of which have total attenuation cross sections equivalent to those of water. The effect of (n, γ) heating in these three materials is small but the larger effect of (n, γ) heating in the tungsten emitter (adjacent to the Teflon capsule) is felt in the T. L. D. simply through the increased gamma field produced in the tungsten. An estimate of (n, γ) heating in tungsten at the face of the emitter was given in table VI. By converting these values to heating in low-z material, the maximum contribution to heating in the T. L. D. at position 1 was estimated as shown in table VI. The comparison at position 1 should be made between directly measured values and calculated values of gamma heating in water (with almost identical μ_e to LiF, Teflon and Al) plus the (n, γ) contribution for water.

At the gap, the powder is completely surrounded by metal, tungsten on one side and niobium on the other. Here the measured values are certainly representative of gamma heating in the two metals with the total effect of the (n, γ) contribution in tungsten, as evaluated in table VI, being recorded in the T. L. D. For comparison with experiment, the calculated values used herein are an average of gamma heating in tungsten and in niobium at the gap with the (n, γ) contribution from tungsten (as in table VI) added.

TABLE VII. - COMPARISON OF RESULTS

| Core condition | Diode elevation, in. | Emitter thickness, cm | Gamma heating, W/g, at position - | | | | | |
|----------------|----------------------|-----------------------|-----------------------------------|----------|----------------|----------|----------------|----------|
| | | | 1, in water | | 2, in W + Nb | | 3, in W + Nb | |
| | | | Calculated (a) | Measured | Calculated (a) | Measured | Calculated (a) | Measured |
| BOL | 0 | 1/3 | 12.07 | 12.24 | 9.27 | 12.58 | 10.31 | 12.82 |
| | 0 | 2/3 | 12.34 | 11.98 | 9.42 | 11.60 | 10.97 | 12.43 |
| | 0 | 1 | 13.37 | 12.63 | 8.12 | 7.74 | 10.54 | 9.35 |
| | 4 | 2/3 | 8.08 | 9.20 | 6.24 | 8.16 | 7.18 | 8.90 |
| | 8 | 2/3 | 4.50 | 5.20 | 3.34 | 4.90 | 3.97 | 5.54 |
| EOL | 0 | 2/3 | 13.84 | 12.59 | 10.56 | 10.34 | 12.26 | 11.26 |
| | 4 | 2/3 | 12.19 | 11.06 | 9.35 | 9.15 | 10.67 | 9.96 |
| | 8 | 2/3 | 8.46 | 8.95 | 6.60 | 7.43 | 7.50 | 8.41 |

^aAll values include the appropriate (n, γ) contribution.

With these concepts in mind, a direct comparison of experimental and calculated results is presented in table VII. All calculated values, fall within the ± 25 percent error bars of the measured values. In general, the data illustrate these logical trends, and experiment supports the calculated results.

CONCLUDING REMARKS

Herein it has been demonstrated that judicious application of the QAD-P5 program can yield reliable evaluations of gamma heating near a high-flux source such as the Plum Brook reactor. Of course, the accuracy of the results depends greatly on the accuracy of input (i.e., cross sections, neutron flux, and buildup factors). However, the low buildup factors (2 to 3) generated in this problem reduce considerably the anticipated inaccuracies usually associated with buildup factor methods. For a valid comparison between calculation and experiment, it was necessary to consider the (n, γ) contribution in the tungsten and some subtle effects of environment on T. L. D. readings. The application of QAD-type calculations to other detectors in a given core becomes simpler and more reliable once the technique and inputs are tested by one experimental example.

Lewis Research Center,

National Aeronautics and Space Administration,

Cleveland, Ohio, December 1, 1967,

120-27-05-09-22.

APPENDIX - AREA-WEIGHTING METHOD

Area weighting is a method of obtaining average values of gamma heating from the continuously varying flux data. The gamma-heating value obtained from the QAD program is shown schematically in figure 12 as varying from some minimum at the center of the

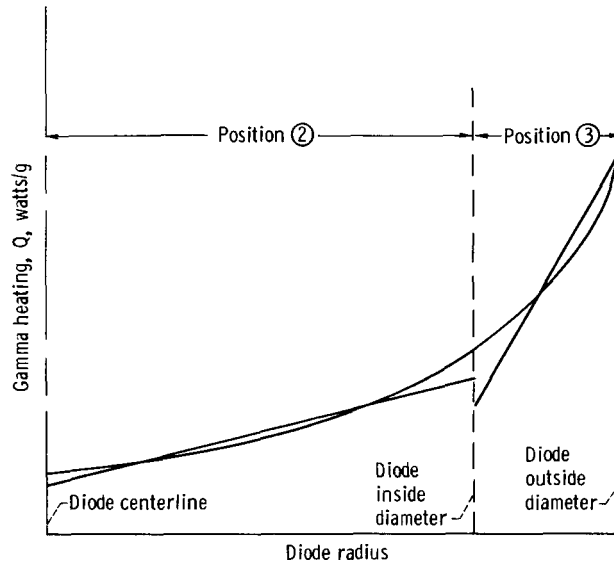


Figure 12. - Typical gamma heating profile.

diode to some maximum at the outside diameter. The two dashed vertical lines denote the boundaries of the inside and outside dosimeter areas. In order to compare calculated values with dosimeter values, the average flux under the calculated curve in each region must be determined. To do this, the Q curve is approximated in each region by a linear function

$$Q(r) = mr + b \quad (1)$$

where

m slope

b intercept at $r = 0$

Then the total heating is determined by integrating this equation between r_o and r_i for the region in question.

The area-weight gamma heating can be specified as

$$\bar{Q} = \int_{r_i}^{r_o} \frac{\phi(r) 2\pi r dr}{\pi(r_o^2 - r_i^2)} \quad (2)$$

$$\bar{Q} = \frac{2 \left(\frac{br^2}{2} + \frac{mr^3}{3} \right) \Big|_{r_i}^{r_o}}{r_o^2 - r_i^2} \quad (3)$$

$$\bar{Q} = \frac{br_o^2 - br_i^2 + \frac{2}{3} m (r_o^3 - r_i^3)}{r_o^2 - r_i^2} \quad (4)$$

$$\bar{Q} = b + \frac{2}{3} m \left(\frac{r_o^2 + r_o r_i + r_i^2}{r_o + r_i} \right) \quad (5)$$

For the inner region (region 2), where $r_i = 0$ and $r_o = 0.90$ centimeter,

$$\bar{Q}_2 = b + \frac{2}{3} m(0.90) \quad (6)$$

For the outer region (region 3), where $r_i = 0.90$ centimeter and $r_o = 1.258$ centimeters,

$$\bar{Q}_3 = b + \frac{2}{3} m(1.64)$$

By definition, $\bar{Q} = b + m\bar{r}$, where \bar{r} is the radial distance to the point where the average gamma-heating value for that region is found. Rewriting equation (6) yields

$$\bar{Q}_2 = \bar{Q}_2 - m(\bar{r}_2) + \frac{2}{3} (0.90)m \quad (7)$$

For region 2, \bar{r}_2 may be written $\bar{r}_2 = 0.60$ centimeter. Similarly from equation (7), \bar{r}_3 may be written as $\bar{r}_3 = 1.09$ centimeters. A straight line is drawn for each region approximating the continuously varying function, and the average value of gamma heating for that region is picked off at the appropriate r for that region.

REFERENCES

1. Forman, R.: Electrical Properties of Inert Gas Plasmas Generated in Thermionic Cold-Cathode Diodes by Radiation in a Nuclear Reactor. *J. Appl. Phys.*, vol. 36, no. 4, Apr. 1965, pp. 1344-1350.
2. Kondratiev, F. V.; Sintertin, G. V.; and Tikchonov, V. F.: Influence of Reactor Radiation on the Operation of Caesium Diode. *International Conference on Thermionic Electrical Power Generation*. Institute of Electrical Engineers, London, 1967, pp. 80-83.
3. Curie, Daniel (G. F. J. Garlick, trans.): *Luminescence in Crystals*. John Wiley & Sons, Inc., 1963.
4. Cameron, J. R.; Zimmerman, D.; Kenney, G.; Buch, R.; Bland, R.; and Grant, R.: Thermoluminescent Radiation Dosimetry Utilizing LiF. *Health Phys.*, vol. 10, no. 1, Jan. 1964, pp. 25-29.
5. Evans, Robley D.: *The Atomic Nucleus*. McGraw-Hill Book Co., Inc., 1955, pp. 623-625.
6. Malenfant, Richard E.: QAD, A Series of Point-Kernel General-Purpose Shielding Codes. Rep. No. LA-3573, Los Alamos Scientific Lab., Apr. 5, 1967.
7. Lahti, Gerald P.: QADHD Point-Kernel Radiation Shielding Computer Code to Evaluate Propellant Heating and Dose to Crew During Engine Operation. NASA TM X-1397, 1967.
8. Anon.: Reactor Physics Constants. Rep. No. ANL-5800, Argonne National Lab., July 1, 1958, sec. 7.
9. Watson, Clayton W., ed.: *Nuclear Rocket Propulsion*. University of Florida, 1964.
10. Celnik, J.; and Spielberg, D.: Gamma Spectral Data for Shielding and Heating Calculations. Rep. No. UNC-5140 (NASA CR-54794), United Nuclear Corp., Nov. 30, 1965.
11. Groshev, L. V.; and Demidov, A. M.: Gamma-Ray Spectrum of the IRT Reactor. *Soviet J. Atomic Energy*, vol. 7, no. 3, Mar. 1961, pp. 748-749.
12. Bjarngard, Bengt E.; McCall, Richard C.; and Bernstein, Irving A.: Lithium Fluoride - Teflon Thermoluminescence Dosimeters. *Thermoluminescent Dosimetry*. Frank H. Attix, ed., A.E.C., 1967, pp. 308-316.
13. Storm, M. L.; Hurwitz, H. Jr.; and Roe, G. M.: Gamma-Ray Absorption Distribution for Plane, Spherical, and Cylindrical Geometries. Rep. No. KAPL-783, Knolls Atomic Power Plant, July 24, 1952.

POSTMASTER: If Undeliverable (Section 158
Postal Manual) Do Not Return

"The aeronautical and space activities of the United States shall be conducted so as to contribute . . . to the expansion of human knowledge of phenomena in the atmosphere and space. The Administration shall provide for the widest practicable and appropriate dissemination of information concerning its activities and the results thereof."

—NATIONAL AERONAUTICS AND SPACE ACT OF 1958

NASA SCIENTIFIC AND TECHNICAL PUBLICATIONS

TECHNICAL REPORTS: Scientific and technical information considered important, complete, and a lasting contribution to existing knowledge.

TECHNICAL NOTES: Information less broad in scope but nevertheless of importance as a contribution to existing knowledge.

TECHNICAL MEMORANDUMS: Information receiving limited distribution because of preliminary data, security classification, or other reasons.

CONTRACTOR REPORTS: Scientific and technical information generated under a NASA contract or grant and considered an important contribution to existing knowledge.

TECHNICAL TRANSLATIONS: Information published in a foreign language considered to merit NASA distribution in English.

SPECIAL PUBLICATIONS: Information derived from or of value to NASA activities. Publications include conference proceedings, monographs, data compilations, handbooks, sourcebooks, and special bibliographies.

TECHNOLOGY UTILIZATION PUBLICATIONS: Information on technology used by NASA that may be of particular interest in commercial and other non-aerospace applications. Publications include Tech Briefs, Technology Utilization Reports and Notes, and Technology Surveys.

Details on the availability of these publications may be obtained from:

SCIENTIFIC AND TECHNICAL INFORMATION DIVISION
NATIONAL AERONAUTICS AND SPACE ADMINISTRATION

Washington, D.C. 20546